Thermal Imaging as a Biometrics Approach to Facial Signature Authentication

Ana M. Guzman, Mohammed Goryawala, Jin Wang, Armando Barreto, Jean Andrian, Naphtali Rishe, and Malek Adjouadi

***Abstract*—A new thermal imaging framework with unique feature extraction and similarity measurements for face recognition is presented. The research premise is to design specialized algorithms that would extract vasculature information, create a thermal facial signature, and identify the individual. The proposed algorithm is fully integrated and consolidates the critical steps of feature extraction through the use of morphological operators, registration using the Linear Image Registration Tool, and matching through unique similarity measures designed for this task. The novel approach at developing a thermal signature template using four images taken at various instants of time ensured that unforeseen changes in the vasculature over time did not affect the biometric matching process as the authentication process relied only on consistent thermal features. Thirteen subjects were used for testing the developed technique on an in-house thermal imaging system. The matching using the similarity measures showed an average accuracy of 88.46% for skeletonized signatures and 90.39% for anisotropically diffused signatures. The highly accurate results obtained in the matching process clearly demonstrate the ability of the thermal infrared system to extend in application to other thermal-imaging-based systems. Empirical results applying this approach to an existing database of thermal images prove this assertion.**

***Index Terms*—Biometric, face recognition, image registration, image segmentation, thermal imaging.**

I. Introduction

IDENTIFICATION systems rely on three key elements: 1) attribute identifiers (e.g., Social Security Number, driver's license number, and account number), 2) biographical identifiers (e.g., address, profession, education, and marital status), and 3) biometric identifiers (e.g., fingerprint, iris, voice, and gait). It is rather easy for an individual to falsify attribute and biographical identifiers; however, biometric identifiers depend on intrinsic physiological characteristics that are difficult to falsify or alter. Applications for face recognition can be found in the areas of entertainment, smart cards, information security, law enforcement, medicine, and security [1], [2]. Diverse techniques and systems have been created for face detection in areas that use cameras in the visible spectrum. Machine recognition of human faces has experienced great strides but remain challenged by intricate issues related to light variability [3] and other factors like difficulty in detecting facial disguises.

The use of thermal mid-wave infrared (MWIR) portion of the electromagnetic (EM) spectrum solves the problem of light variability. Also, any foreign object on a human face such as a fake nose could be detected, as foreign objects have a different temperature range than that of human skin. Due to these benefits, a lot of effort has been aimed at developing human face recognition systems in the MWIR spectrum. However, since cameras in the MWIR portion of EM spectrum are available at a much higher cost than their visible band counterparts, much of the research done in human face recognition in the MWIR spectrum is still in its infancy.

In recent years, researchers have realized the potential of thermal MWIR imagery for human identification using the vein structure of hands [4], [5], finger vein patterns [6], [7], and vein structure of the human face [8]. Also thermal images have been used to identify the affective state of humans [9]. Moreover, the fusion of visual and thermal face images has been used in the face recognition field [10]. The work performed by the research group in [11] represents the first attempt at developing an algorithmic approach to face recognition using physiological information obtained from MWIR images.

In this study, we extend this research by presenting an integrated approach that consolidates unique algorithms at extracting thermal imaging features, producing templates that rely on the most consistent features, and matching these features through newly developed similarity measures for authentication. Given the complex nature of human vasculature, this approach to face recognition using MWIR imaging is checked against another existing database to prove the reliability of the algorithms designed for feature extraction, template generation, and authentication through similarity measures.

II. Materials and Methods

The work presented in this study consists of three major modules: 1) collection of MWIR images, 2) feature extraction, and 3) feature matching. In each of these modules, different instructive steps and safeguards starting from camera calibration to facial thermal signature extraction are taken to ensure that authentication is made through features that are consistent through several image acquisition times and are therefore more likely to be part of the vasculature of the individual.

Manuscript received November 3, 2011; revised March 20, 2012 and June 6, 2012; accepted June 25, 2012. Date of current version February 4, 2013. This work was supported by the National Science Foundation under Grants CNS-1042341, CNC-0959985, and HRD-0833093F.

A. M. Guzman, J. Wang, A. Barreto, J. Andrian, N. Rishe, and M. Adjouadi are with the Department of Electrical Engineering, Florida International University, Miami, FL 33174 USA (e-mail: ana.guzman2@fiu.edu; jwang006@fiu.edu; barretoa@fiu.edu; jean.andrian@fiu.edu; rishe@fiu.edu; adjouadi@fiu.edu).

M. Goryawala is with the Department of Biomedical Engineering, Florida International University, Miami, FL 33174 USA (e-mail: mgory001@fiu.edu).

Digital Object Identifier 10.1109/TITB.2012.2207729

A. Collection of MWIR Images

Data collection was accomplished using the Merlin MWIR camera system which operates in the MWIR of the EM spectrum. For this study, we collected thermal infrared images from 13 different subjects. The Merlin MWIR camera was placed on a tripod at a distance of 1 m from the subject who is asked to sit on a fixed chair to facilitate the picture-taking process. The recording of the thermal infrared images was done in a room with an average room temperature of 23 °C. Each subject was asked to sit straight in front of the thermal infrared camera and asked to look straight into the lens and a snapshot of their frontal view was taken. This process was repeated at least three more times in different days and times of the day to take into consideration subtle variations that may occur over time. The time gap for acquisition of the images among and within subjects varied from a period of a week for some subjects up to three months for others.

B. Feature Extraction

Once a thermal camera is calibrated, one of the most challenging tasks of any biometric system is the feature extraction process, which in the final analysis should mimic in the best way possible the human facial vasculature. The premise is that facial skin temperature is closely related to the underlying blood vessels; thus by obtaining a thermal map of the human face, we can also extract the pattern of the blood vessels just below the skin. Thermal feature extraction from facial images was attained by performing morphological operations such as opening and top-hat segmentation to yield thermal signatures for each subject. Four thermal images taken over a period of six months were used to generate a thermal signature template for each subject to contain only the most prevalent and consistent features. In this study, consistent features are defined as those features which are present in three or more thermal signatures obtained from an individual's images taken at different times. A detailed explanation of extracting these consistent features is provided in Section II-B2e.

An important contribution at this stage of the process is in the way unique templates are generated for each individual, which through anisotropic diffusion and unique registration processes create facial signatures that encompass the most consistent features recorded over time. This is an essential step that ensures that facial authentication is carried out with success. Fig. 1 displays the flowchart of the entire procedure showing the steps required for the feature extraction process to generate features templates which will then be matched against any facial signature as input to the system.

1) Thermal Infrared Image Registration: Image registration is a challenging task in the field of image processing. Various techniques are available for image registration for medical images and for images in biometric applications [12]–[14]. The intrasubject image registration of the acquired thermal infrared images was performed using the FMRIB Software Library (FSL). The image registration process was achieved using the Analysis Group at the Oxford Center for functional magnetic resonance imaging (MRI) of the Brain's (FMRIB's) Linear Image Registration Tool (FLIRT), assuming the rigid body model option for 2-D image registration. FLIRT has been shown to be significantly faster and accurate in image registration as compared to other techniques such as simulated annealing of the genetic algorithms for MRI applications [15], [16]. However, the specific use of FLIRT for registering thermal facial images as presented in this study has not been addressed in the literature to the best of our knowledge.

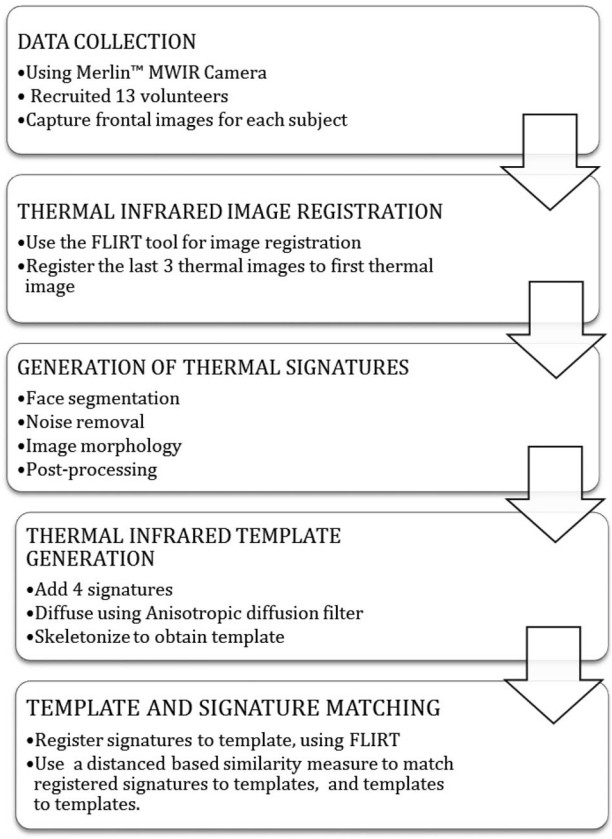

Fig. 1. Flow diagram of the entire thermal-signature-based biometric recognition approach.

Four images from each subject were used in the registration process, whereby one was chosen as the reference image and the rest were registered to the reference image. The thermal image of the subject is taken at different times, and therefore, slight lateral and vertical shifts in the position of the subject relative to the camera's position are experienced. The purpose of the registration process is to account for any lateral and/or vertical movement from the subject that could have taken place during data collection. This simplifies the overlay of the signatures and templates, and makes similarity measurements more meaningful.

The FLIRT registration of images greatly depends on the parameters chosen for the registration task. The various parameters that need to be addressed are 1) cost function, 2) degrees of freedom (DOF), and 3) interpolation. The choice of the cost function depends on the nature of the image to be registered

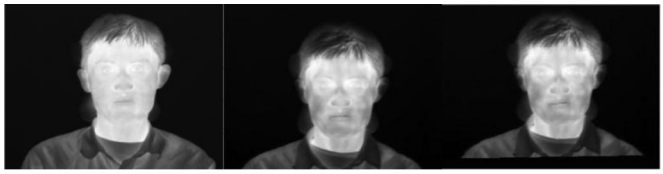

(a) (b) (c)

Fig. 2. Results of thermal image registration procedure. (a) Reference image. (b) Image to be registered. (c) Registered image after using the developed registration technique.

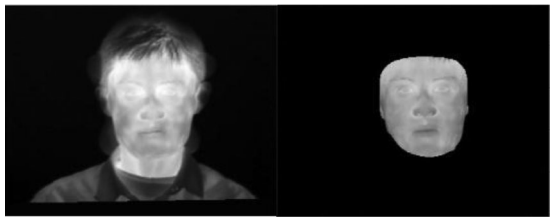

Fig. 3. Results of the segmentation process showing the original thermal image and the face segmented image.

in terms of size and gray scale, relative to other images. Also, since both the input and the reference images in this case are of the same modality, a within-modality cost function has to be employed to obtain better results. It was found that for thermal images under consideration, the "mutual information" cost function gave us the best registration results. Mutual information formulation used for the registration of the thermal images was first suggested in [17] and [18]. The mutual information is the combination of three different entropies. These include the separate entropies of the two images to be registered as well as their joint entropy.

Four DOF are chosen for the study: one each for the two dimensions of the image, one for rotation, and one for the scaling. The FLIRT algorithm is employed thus using 4 DOF to achieve a complete registration between the two images. The interpolation step of the process is only used for the final transformation, not in the registration calculations. Various types of interpolations can be used, but since the images are fairly aligned with only slight shifts in position, a nearest neighbor interpolation was found to be sufficient. Fig. 2 shows the results of the registration process for one of the subjects. Notice how the registered image is shifted up in order to correctly register the image to the reference image.

2) Thermal Signature Extraction: After registering the thermal images for each subject, we proceeded to extract the thermal signature in each image. The thermal signature extraction process has four main sections: face segmentation, noise removal, image morphology, and postprocessing.

a) Face segmentation: In this step, the face of the subject was segmented from the rest of the image. The segmentation process was achieved by implementing the technique of localizing region-based active contours in which typical region-based active contour energies are localized in order to handle images with nonhomogeneous foregrounds and backgrounds [19], [20]. The face region segmented here does not take into consideration the neck of the person. This is achieved by localizing the contouring algorithm to a neighborhood around the point of interest with a localization radius of 5 pixels. Since some subjects tended to wear clothing that obstructed the neck region area, we opted not to include that region for uniformity in the segmentation process as well as in performing the similarity measurements to involve only the face.

Let $\Psi = \{x|\Phi(x) = 0\}$ be a closed contour of interest. The interior of the closed contour Ψ is expressed in terms of the smoothed approximation of the signed distance function given as

$$\Phi(x) = \begin{cases} 1, & \Phi(x) < -\varepsilon \\ 0, & \Phi(x) > \varepsilon \\ \frac{1}{2}\left\{1 + \frac{\Phi}{\varepsilon} + \frac{1}{\pi}\sin\frac{\pi\Phi(\mathrm{x})}{\varepsilon}\right\}, & \text{otherwise} \end{cases} \quad (1)$$

where $\Phi(x)$ is a smoothed initial contour and $[-\varepsilon, \varepsilon]$ represents the boundary of the Heaviside function in (1). In reference to (1), the exterior of the closed contour is given as $\{1 - H\Phi(x)\}$.

In order to model the energies of the interior and exterior of the contour for face segmentation purposes, the well-known Yezzi energy is used [21]. The Yezzi energy defines a dual-front active contour, which is widely used for segmentation purposes in cases where the solution may fall in a local minima and yield poor results.

The algorithm operates by first dilating the user-selected initial contour to create a potential localized region *R* for finding the optimal segmentation. Thus

$$R = \Phi \oplus S \quad (2)$$

where *S* is a spherical structuring element of the localization radius (i.e., 5 pixels) and $\oplus$ is the dilation operator.

The algorithm proceeds by evolving the inner and outer boundaries of *R* to reach minima where the inner and outer boundary contours intersect after applying a single iteration of the algorithm called the dual-front active contour region-growing technique. The newly formed intersection acts as a new initialization and the process is repeated until the Yezzi energy function is minimum. Fig. 3 shows the original thermal image and the resultant image after the segmentation procedure. It can be seen that the algorithm successfully segments out the face removing the neck and the hair region from the face.

b) Noise removal: After the face was segmented from the rest of the thermal infrared image, we proceeded to remove unwanted noise in order to enhance the image for further processing. A standard Perona–Malik anisotropic diffusion filter [22] is first applied to the entire thermal image.

The significance of the anisotropic diffusion filter in this particular application is to reduce spurious and speckle noise effects seen in the images and to enhance the edge information for extracting the thermal signature. For the diffusion filter, a 2-D network structure of eight neighboring nodes (north, south, east, west, northeast, northwest, southeast, and southwest) is considered for diffusion conduction. The conduction coefficient function used for the filter applied on the thermal images aims to

privilege edges over wider regions in order to enhance regions of high thermal activity associated with the thermal signature. Thus, the conduction coefficient function used for the application is given by

$$C(x,\, y,\, t) = \frac{1}{1 + \left(\dfrac{||\nabla I||}{K}\right)^2} \tag{3}$$

where ∇I is calculated for the eight directions and K is the gradient modulus threshold that controls the conduction and avoids the blurring of facial features.

c) Image morphology: Image morphology is a way of analyzing images based on shapes. In this study, we assume that the blood vessels are a tubule-like structure running along the length of the face. The operators used in this experiment are opening and top-hat segmentation, which are detailed next. The effect of an opening operation is to preserve foreground regions that have a similar shape to the structuring element or that can completely contain the structuring element, while eliminating all other regions of foreground pixels. The opening of an image can be described mathematically as follows:

$$I_{\text{open}} = (I \Theta S) \oplus S \tag{4}$$

where I and I_{open} are the face segmented image and the output opened image, respectively; Θ and $\oplus$ are the morphological erosion and dilation operators.

The top-hat segmentation has two versions; for our purpose, we use the version known as white top-hat segmentation as this process enhances the bright objects in the image; this operation is defined as the difference between the input image and its opening. The selection of the top-hat segmentation is based on the fact that we desire to segment the regions associated with those of higher intensity, which demark the facial thermal signature. The task in this step is to enhance the maxima in the image. The top-hat segmented image I_{top} is thus given by

$$I_{\text{top}} = I - I_{\text{open}}. \tag{5}$$

d) Postprocessing: After obtaining the maxima in the image, the skeletonization process is used to reduce the foreground regions into a skeletal remnant that largely preserves the extent and connectivity of the original region. This is a homotopic skeletonization process whereby a skeleton is generated by image morphing using a series if structural thinning elements from the Golay alphabet [23].

Morphological thinning is defined as a hit-or-miss transformation which is essentially a binary template matching where a series of templates L_1 through L_8 are searched throughout the image. A positive search is annotated as 1 and a miss as 0. This annotation is the result of the following mathematical expression:

$$I_{\text{skel}} = I_{\text{top}} | (I_{\text{top}} \underline{\hat{x}} L_i) \tag{6}$$

where $\underline{\hat{x}}$ is the hit-or-miss operator and L_i is the set of structuring elements L_1 through L_8. The first two structuring elements used for the skeletonization process are shown as follows:

$$L_1 = \begin{bmatrix} 1 & 1 & 1 \\ 0 & 1 & 0 \\ 0 & 0 & 0 \end{bmatrix}, \quad L_2 = \begin{bmatrix} 0 & 1 & 0 \\ 0 & 1 & 1 \\ 0 & 0 & 0 \end{bmatrix}. \tag{7}$$

The rest of the six structuring elements can be obtained by rotating both the masks L_1 and L_2 by 90°, 180°, and 270°. Fig. 4 shows the resultant image after the postprocessing approach. The image shown in Fig. 4(b) is referred to here as the thermal signature of that particular subject.

(a) (b)

Fig. 4. Result of the signature extraction procedure. (a) Original thermal image. (b) Thermal signature.

(a) (b) (c)

Fig. 5. Generation of thermal signature template. (a) Resultant image of addition of four thermal signatures. (b) Results of applying anisotropic diffusion on summed image. (c) Thermal signature template of the subject.

e) Generation of thermal signature template: Thermal signatures in an individual vary slightly from day to day due to various reasons like exercise, environmental temperature, weight, health of the subject, temperature of the imaging room, and many more [24]. Taking into consideration the various factors that may affect the thermal signature, the proposed approach relies on establishing a thermal signature template that preserves those characteristics in a person's thermal signature that are consistent over time.

The generation of a thermal signature template consists of taking the extracted thermal signatures for each subject and adding them together. The resulting image is a composite of four thermal signature extractions, each one slightly different from the other. The goal is to keep the features that are present in all the images as the dominant features that otherwise define best the individual signature. We then apply an anisotropic diffusion filter to the result of the added thermal signatures in order to fuse the predominant features.

These different steps together with the final template that is sought are illustrated in Fig. 5. For all future testing purposes, a database of the templates is created against which any newly acquired thermal signature image is tested.

Fig. 6 shows some illustrative examples on how the thermal signature templates are overlaid on the thermal image of the corresponding subject.

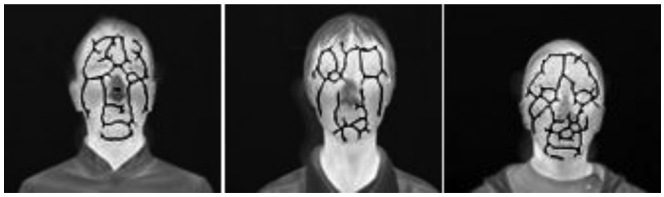

Fig. 6. Illustrative thermal templates overlaid on the thermal image of the corresponding subject.

C. Distance-Based Similarity Measure for Thermal Infrared Signatures and Template Matching

Similarity measures are widely used in applications like image databases, in which a query image is a partial model of the user's desires and the user looks for images similar to the query image [25], [26]. In our study, we make use of similarity measures because we are attempting to find a thermal infrared template similar to the query thermal infrared signature.

Given a thermal infrared signature *A* (nonreference image), and a thermal infrared template *B* (reference image), the similarity measure between *A* and *B*, denoted by $S(A \rightarrow B)$, is defined as follows:

$$S(A \rightarrow B) = \sum_{i=1}^{h} \frac{1}{h(D_i + 1)} \tag{8}$$

where *1/h* is the weight associated in matching a single feature (or thermal pixel). Parameter *h* denotes the minimum number of feature points found in either *A* or *B*, i.e., $h = \min(N_A, N_B)$, where N_A and N_B are the number of features in *A* and *B*, respectively. Parameter *h* is the maximum number of features that we could obviously match. The parameter D_i is the minimum Euclidean or Manhattan distance between the *i*th feature point in *B* and its closest feature point in *A*. In finding D_i, the distance of all features in *A* to those in *B* are computed, thus creating a vector containing *h* Euclidean distances for every feature point. The two features that correspond to the minimum distance in the vector are then matched; this process continues until all *h* features are considered. Also, when two or more features in *A* match the same feature in *B*, it means that two or more features in *A* are equidistant to *B*. In such a case, we decided to take the first feature in *A* and match it to *B*.

It is to be noted that the similarity measure defined in the study obeys the property of symmetry as long as the image with the minimum number of features (*h*) is referred to as the reference window or reference image.

In addition to computing similarities with the skeletonized templates of the subject, we calculated the similarities between the diffused versions of the signatures and templates. The motive behind generating a diffused template and comparing to it was to see if minor errors resulting due to misalignment of the images have an impact on the similarities.

III. Results

To demonstrate the distinctiveness of the generated templates for each of the subject, we calculated the similarity between the various templates. Table I shows in column 2 the results of comparing Template of subject 10 to the other templates. It is seen that a similarity of unity is obtained when template of subject 10 is matched to itself (intrasubject), which is expected. It is also seen that when this template is matched to the template of any other subject (intersubject), a similarity value of no higher than 0.34 is obtained which clearly demonstrates the distinctiveness between the templates of the 13 subjects. It should, however, be noted that the distinctiveness of the templates under investigation has to be verified with a larger number of subjects in future studies. The third column of Table I provides similarity results of the closest nonmatch for each template in column 1.

TABLE I
Similarity Values for Skeletonized Template Versus Template Matching

Template	Similarity Value Template Subject 10 as reference.	Similarity Value for Closest Non-match
Subject 10	1.0000	0.3414 (Subject 11)
Subject 11	0.3414	0.3107 (Subject 2)
Subject 2	0.3082	0.3480 (Subject 11)
Subject 3	0.3057	0.3114 (Subject 1)
Subject 9	0.2872	0.3513 (Subject 11)
Subject 6	0.2841	0.3659 (Subject 1)
Subject 8	0.2825	0.3686 (Subject 1)
Subject 4	0.2815	0.3239 (Subject 6)
Subject 13	0.2832	0.3247 (Subject 4)
Subject 1	0.2724	0.3614 (Subject 6)
Subject 7	0.2649	0. 3280 (Subject 3)
Subject 12	0.2640	0.3554 (Subject 1)
Subject 5	0.2609	0.3239 (Subject 9)

TABLE II
Intersubject Similarities Computed on Comparing Skeletonized Signature of Subject 12 to Other Skeletonized Database Templates

Signature	Similarity Value Template Subject 12 as reference.
Subject 12	0.6158
Subject 1	0.3420
Subject 6	0.3306
Subject 7	0.3110
Subject 8	0.3049
Subject 5	0.2880
Subject 9	0.2876
Subject 3	0.2859
Subject 4	0.2806
Subject 13	0.2698
Subject 10	0.2597
Subject 11	0.1983
Subject 2	0.1975

Table II shows the results of matching a particular facial thermal signature to all the templates in the database. For illustrative purposes, Table II provides the results obtained by matching the signatures from all subjects to the facial thermal template of subject 12. As seen in Table II, the similarity of match is the highest when the signature of subject 12 is compared to its own template as compared to others. This is considered a positive match; however, if the similarity with any other subject's template was found to be higher than that of its own template, then it is considered a negative match.

Fig. 7(a) illustrates the positive match between template and signature of subject 12, the template is shown in white and the

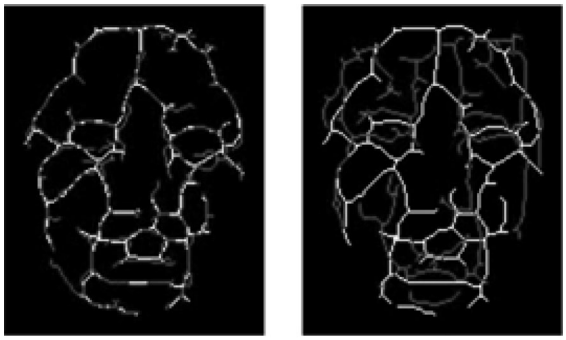

(a) (b)

Fig. 7. Illustration of (a) positive match for subject 12 and (b) negative match for subject 2. Templates are shown in white and signatures in gray.

TABLE III
INTERSUBJECT SIMILARITIES COMPUTED ON DIFFUSED SIGNATURE OF SUBJECT 12 AND THE DIFFUSED TEMPLATES OF ALL 13 SUBJECTS

Signature	Similarity Value Template Subject 12 as reference.
Subject 12	0.7569
Subject 1	0.3915
Subject 7	0.3783
Subject 9	0.3507
Subject 6	0.3462
Subject 5	0.3335
Subject 3	0.3176
Subject 8	0.3143
Subject 13	0.3107
Subject 4	0.3023
Subject 10	0.2994
Subject 2	0.2320
Subject 11	0.2032

signature in gray. Fig. 7(b) shows a negative match between the template of subject 12, shown in white, and the signature of subject 3 shown in gray.

Table III presents the same information as in Table II except that instead of skeletonized signatures and template, diffused signatures and templates were used while computing the similarities. It is seen that as expected the similarity between the signature of subject 12 and template of subject 12 is the highest; however, the value is greater than that obtained using skeletonized templates. Such an improvement in the similarity measure was seen on comparison of every signature. It was found that an average 18.9% improvement in the similarity measure was obtained when using diffused templates. The similarity of nonmatches also increased when using diffused template but only on an average of 12.64%. Table IV presents the overall results for the comparison of the signatures to the database templates. Four signatures S-1 to S-4 for each subject were compared to the database template, and the average accuracy of the match is reported for both the skeletonized and the diffused templates.

At this juncture, the results presented used solely Euclidean distances. We also calculated the similarities based on the Manhattan or City block distances. Table V presents the results obtained when comparing four signatures taken over time with the templates in the database using Manhattan distance.

TABLE IV
ACCURACY OF MATCHING FOR FOUR DISTINCT SIGNATURES TAKEN AT DIFFERENT TIME TO THE SKELETONIZED AND DIFFUSED TEMPLATES IN THE DATABASE USING EUCLIDEAN DISTANCES

D_i , Euclidean	S-1	S-2	S-3	S-4	AVG.	σ
Accuracy (skeletonized)	92.31%	76.92%	92.31%	92.31%	88.46%	7.69
Accuracy (diffused)	92.31%	84.61%	92.31%	92.31%	90.39%	3.85

TABLE V
ACCURACY OF MATCHING FOR FOUR DISTINCT SIGNATURES TAKEN AT DIFFERENT TIME TO THE SKELETONIZED AND DIFFUSED TEMPLATES IN THE DATABASE USING MANHATTAN DISTANCES

D_i , Manhattan	S-1	S-2	S-3	S-4	AVG.	σ
Accuracy (skeletonized)	100%	76.92%	92.31%	92.31%	90.39%	9.68
Accuracy (diffused)	100%	76.92%	92.31%	92.31%	90.39%	9.68

TABLE VI
ACCURACY OF MATCHING FOR DISTINCT SIGNATURES TAKEN AT DIFFERENT TIME TO THE SKELETONIZED TEMPLATES GENERATED USING TWO OR THREE THERMAL SIGNATURES IN THE DATABASE USING EUCLIDEAN DISTANCES

	S-1	S-2	S-3	S-4	Avg.	σ
Template2S	61.54%	84.62%	92.31%	-	79.49%	16.01
Template3S	92.31%	61.54%	84.62%	92.31%	82.69%	14.56

A paired two-tail student T-test was employed to determine if the accuracies obtained using the different distance methods are statistically different. It was found that the two distance measures do not yield statistically different results ($p = 0.39$).

In order to ascertain if the developed thermal imaging technique was sensitive to the number of images that are used toward the generation of the thermal signature template, we carried out the entire detection process to using only two or three thermal signatures (instead of four) for the creation of the thermal signature template. Table VI provides the accuracies obtained in these scenarios using the Euclidean distances. In Table VI, Template 2S and Template 3S denote the thermal signature templates obtained using two and three thermal signatures, respectively. Recall that the thermal signatures used for the generation of the thermal signature template are obtained from images taken at distinct intervals of time to accommodate for slight discrepancies in the thermal signatures.

It is seen from Table VI that using Template 2S, a low accuracy score for S-1 was observed, where five mismatches were observed. From the above analysis, it is seen that the average accuracy reduces as the number of images used for the creation of the thermal signature template are reduced. Fig. 8 displays the trend in the accuracy as a function of the number of images used for the generation of the template.

Once the merit of these similarity measures were confirmed within our database of subjects, other experiments were then conducted involving subjects from a different database provided by the University of Notre Dame [27], [28], the thermal images in this database, which consisted of 83 subjects each with four different poses, were collected using a long-wave infrared (LWIR), noncooled camera from Indigo systems, the dataset is

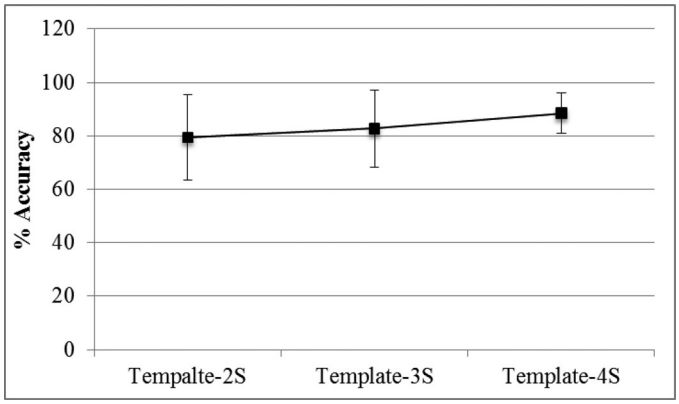

Fig. 8. Accuracy of matching for distinct signatures taken at different time to the skeletonized templates generated using two, three, or four thermal signatures in the database using Euclidean distances. The error bars in the figure denote the respective standard deviations.

TABLE VII
ACCURACY MATCHING FOR FOUR DISTINCT SKELETONIZED SIGNATURE SETS AND TEMPLATES FOR 25 SUBJECTS IN THE C-X1 DATABASE

	S-1	S-2	S-3	S-4	AVG.	σ
Euclidean (skeletonized)	84%	72%	64%	48%	67%	15.1
Manhattan (skeletonized)	84%	68%	72%	56%	70%	11.55

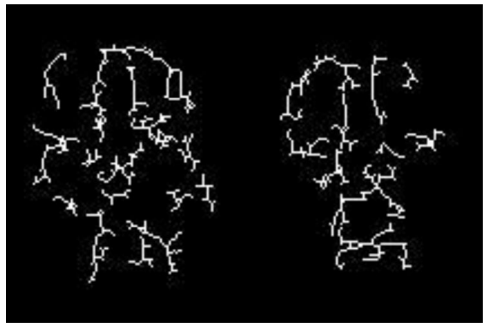

Fig. 9. Thermal signatures of two subjects in dataset C-X1.

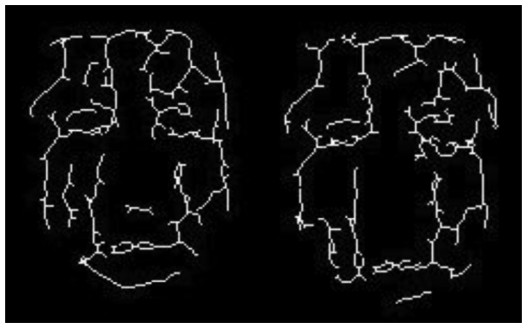

Fig. 10. Thermal signatures of a subject in dataset C-X1 and whose similarity values result in a positive match to its template.

referred to as Collection X1 (C-X1). We could have used the entire dataset, but for illustrative purposes, we have selected 25 different subjects and four neutral pose thermal images with similar face alignment for each subject. We applied the already described feature extraction algorithm to these new thermal images. We created a template from the facial signatures obtained for comparative purposes.

The challenge is viewed in this instance in the fact that the signatures obtained were in our opinion too noisy and may include features that are not necessarily part of the facial signature. Nonetheless, our results are quite robust in including their database to prove the validity of the proposed approach, including the merit of the similarity measure. Using the Euclidean-based and Manhattan-based similarity measure, we obtained results for comparing the templates and signatures from the C-X1 dataset to the templates in our database. When we compared template to template using the Euclidean- and Manhattan-based similarity measure, the template matching was 100% accurate and none of the templates in our database were matched to the new templates from the C-X1 dataset and vice versa. However, when it came to match signatures to templates, the new signatures were often mismatched with the templates in our database; the signatures in our database were never matched to the C-X1 templates. We chose randomly 25 subjects from the C-X1 database and generated thermal signatures and templates for each subject; we proceeded to compute the similarity measure for template and signature matching in the same fashion as with the subjects in our database. Table VII presents the accuracy results obtained for skeletonized signatures and templates using the Euclidean- and Manhattan-based similarity measure.

The accuracy results obtained using skeletonized templates and signatures for the subjects in the C-X1 database are lower than the accuracy results obtained using our own database. The average accuracy for subjects in C-X1 is 67% and 70% for Euclidean- and Manhattan-based similarity measure, respectively, whereas the average accuracy for subjects in our database is 88.46% and 90.39% for the Euclidean- and Manhattan-based similarity measure, respectively. The mismatch is inherent in the quality of the images. In communication with this research group, we were informed that the images in C-X1 contain raw measurements values from the sensor. Although the sensor is capable of being radiometrically calibrated, the authors [27], [28] did not attempt to establish lookup tables that compute temperature from the sensor response, so the values provided in each LWIR thermograph is treated as an arbitrary temperature-correlated unit. The dataset in C-X1 also lacks nonuniformity correction (NUC); this is the correction of the nonuniform spread in gain and offset of the FPA detectors. Our method relies on the temperatures detected on the surface of the human skin, so it is of great importance that calibration and NUC are performed in the infrared system. Typical thermal signatures of the C-X1 database are illustrated in Fig. 9 to demonstrate the complex nature of such signatures.

In Fig. 10, we present two thermal signatures of subject 25 whose similarity results in a positive match to its template. In Fig. 11, we present the overlay of the template and signature for the same subject as in Fig. 10, the template is shown in white and the signature is shown in gray. Finally, we present in Fig. 12 the overlay of the template and signature of subject 11 whose similarity value resulted in a negative match. In this case,

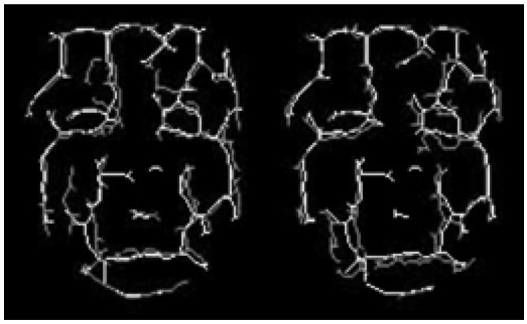

Fig. 11. Overlay of Template (white) and the signatures (gray) for the subject shown in Fig. 10.

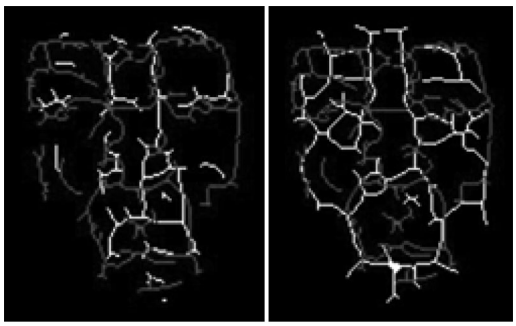

(a) (b)

Fig. 12. Overlay of templates (white) and signatures (gray) whose similarity values produced a negative match. The signature in (a) is subject 11 and in (b) is subject 20.

we present in Fig. 12(a) the overlay of the template and signature subject 11; in this case, the similarity value was not high enough to match the signature to its corresponding template; in Fig. 12(b), we present the overlay of the signature of subject 11 and the template of subject 20 to which it was matched due to having the highest similarity between template and signature.

Due to space limitations in the manuscript, we omitted the long tables. These tables provide the complete results for all experimental runs with their respective statistical measures. However, interested readers may obtain the full tables at http://web.eng.fiu.edu/mgory001/SMsTables-Detailed.xls.

IV. Discussion

Thirteen subjects were used to create an in-house database and we successfully obtained the thermal infrared signatures and templates for the subjects using the proposed technique. The matching using the similarity measures showed 88.46% accuracy in case of skeletonized feature signatures and 90.39% accuracy for anisotropically diffused feature signatures using Euclidean distances, whereas an accuracy of 90.39% was obtained using both skeletonized and diffused templates. Such high accuracies in the matching process clearly demonstrate the ability of the developed thermal infrared feature extraction and the distance-based similarity measure for accurate, low cost, and effective subject matching.

It is also seen that using diffused versions of the signatures and templates yielded an 18.9% improvement in the average accuracy (similarity measures). This is a significant improvement in the similarity measures; however, a significant improvement in the detection accuracy was not achieved. Higher similarity measures are always essential in biometric matching processes, and hence, the diffused version of the matching process might be useful. However, if the system is aimed to be more restrictive and stringent, the skeletonized version would be useful.

The novel technique in generating the thermal signature template as illustrated in this paper contributes to the high accuracies obtained in the results. Other studies using thermal images have shown similar accuracies; however, they do not create time-invariant templates as generated here. Our technique, which involved generation of a feature template by combining various images taken over time, ensures that minute changes in the vasculature over time may not impede in the matching process.

Section III also demonstrated that the developed technique resulted in statistically indifferent results when different distance measures are used for the similarity technique. Also, other studies have employed complex fingerprint-matching algorithms to match the thermal signatures. Such techniques are often highly complicated and computationally taxing. The developed technique is simple and fast and yields good accuracies.

We also showed the novel utilization of the FSL tool toward thermal facial feature registration. The technique demonstrated an accurate, fast, and user-initialization independent/free technique for registering thermal facial images. User-initialization independence is of great importance in automating the matching process in case of larger databases.

The generalized structure of the proposed approach, together with the uniqueness in the way thermal signature templates were generated and the similarity measure was formulated, allows this approach to extend to other thermal images and databases. Caution should be taken however on what really constitutes a thermal pixel that is assumed to belong to the vasculature or at least be consistent through time using several thermal images. Thermal infrared image databases are available for research, but the image quality in these databases is unsuitable for our purpose due to the lack of NUC performed before gathering images which leads to erroneous feature extraction; other databases provide images of subjects in the outdoors and who are too far away from the camera to be able to extract a meaningful facial signature. Since these databases were not collected with the purpose of extracting features such as facial blood vessels patterns, future work would be to obtain a greater number of subjects to build a larger database for testing the algorithm.

V. Conclusion

This paper has presented a novel approach for biometric facial recognition based on extracting consistent features from multiple thermal infrared images. The approach used FLIRT for thermal image registration and localized-contouring algorithms to segment the subject's face. A morphological image processing technique was developed to extract features from the thermal images, thus creating thermal signatures; these signatures were used to create templates which were then matched using similarity measures. The matching between templates and

signatures was done twice using a similarity measure based on 1) the Euclidean distance and 2) the Manhattan distance. Using the Euclidean-based similarity measure, we obtain 88.46% accuracy for skeletonized signatures and templates; for anisotropically diffused signatures and templates, we obtain 90.39% accuracy. Using the Manhattan-based similarity measure, we obtain 90.39% accuracy for skeletonized signatures and templates.

We have demonstrated consistency in determining similarity between signatures and their corresponding thermal templates that were *a priori* generated and which consolidated thermal features that were obtained at various time intervals, over a span of six months. This is an important aspect of any biometric matching technique to be able to handle minute or subtle changes in thermal imaging that could complicate the similarity measurements and therefore the identification process. The facial feature template as designed ensures that small changes in the vasculature over time could not impede the matching process, with the premise that those features that belonged to the vasculature should be consistent over time. It is based on this premise that the current authentication process is made to rely only on consistent thermal features as reflected in the thermal facial template.

The accurate results obtained in the matching process along with the generalized design process clearly demonstrate the ability of the thermal infrared system to be used on other thermal-imaging-based systems and their related databases.

REFERENCES

[1] W. Zhao, R. Chellappa, P. J. Phillips, and A. Rosenfeld, "Face recognition: A literature survey," *ACM Comput. Surv.*, vol. 35, pp. 399–459, 2003.

[2] F. W. Prior, B. Brunsden, C. Hildebolt, T. S. Nolan, M. Pringle, S. N. Vaishnavi, and L. J. Larson-Prior, "Facial recognition from volume-rendered magnetic resonance imaging data," *IEEE Trans. Inf. Technol. Biomed.*, vol. 13, no. 1, pp. 5–9, Jan. 2009.

[3] Y. Adini, Y. Moses, and S. Ullman, "Face recognition: The problem of compensating for changes in illumination direction," *IEEE Trans. Pattern Anal. Mach. Intell.*, vol. 19, no. 7, pp. 721–732, Jul. 1997.

[4] C. L. Lin and K. C. Fan, "Biometric verification using thermal images of palm-dorsa vein patterns," *IEEE Trans. Circuits Syst. Video Technol.*, vol. 14, no. 2, pp. 199–213, Feb. 2004.

[5] S. K. Im, H. S. Choi, and S. W. Kim, "A direction-based vascular pattern extraction algorithm for hand vascular pattern verification," *Etri. J.*, vol. 25, pp. 101–108, 2003.

[6] T. Shimooka and K. Shimizu, "Artificial immune system for personal identification with finger vein pattern," *Lect. Notes Comput. Sci.*, vol. 3214, pp. 511–518, 2004.

[7] N. Miura, A. Nagasaka, and T. Miyatake, "Feature extraction of finger-vein patterns based on repeated line tracking and its application to personal identification," *Mach. Vision Appl.*, vol. 15, pp. 194–203, 2004.

[8] P. Buddharaju, I. T. Pavlidis, P. Tsiamyrtzis, and M. Bazakos, "Physiology-based face recognition in the thermal infrared spectrum," *IEEE Trans. Pattern Anal.*, vol. 29, no. 4, pp. 613–626, Apr. 2007.

[9] B. R. Nhan and T. Chau, "Classifying affective states using thermal infrared imaging of the human face," *IEEE Trans. Biomed. Eng.*, vol. 57, no. 4, pp. 979–987, Apr. 2010.

[10] S. Gundimada and V. K. Asari, "Facial recognition using multisensor images based on localized kernel eigen spaces," *IEEE Trans. Image Process.*, vol. 18, no. 6, pp. 1314–1325, Jun. 2009.

[11] I. Pavlidis, P. Tsiamyrtzis, P. Buddhraju, and C. Manohar, "Biometrics: Face recognition in thermal infrared," in *Biomedical Engineering Handbook*, J. Bronzino, Ed. Boca Raton, FL: CRC Press, 2006.

[12] M. Khader and A. Ben Hamza, "Nonrigid image registration using an entropic similarity," *IEEE Trans. Inf. Technol. Biomed.*, vol. 15, no. 5, pp. 681–690, Sep. 2011.

[13] J. A. Zheng, J. Tian, K. X. Deng, X. Q. Dai, X. Zhang, and M. Xu, "Salient feature region: A new method for retinal image registration," *IEEE Trans. Inf. Technol. Biomed.*, vol. 15, no. 2, pp. 221–232, Mar. 2011.

[14] G. van Soest, J. G. Bosch, and A. F. W. van der Steen, "Azimuthal registration of image sequences affected by nonuniform rotation distortion," *IEEE Trans. Inf. Technol. Biomed.*, vol. 12, no. 3, pp. 348–355, May 2008.

[15] M. Jenkinson and S. Smith, "A global optimisation method for robust affine registration of brain images," *Med. Image Anal.*, vol. 5, pp. 143–156, 2001.

[16] M. Jenkinson, P. Bannister, M. Brady, and S. Smith, "Improved optimization for the robust and accurate linear registration and motion correction of brain images," *NeuroImage*, vol. 17, pp. 825–841, 2002.

[17] P. Viola and W. M. Wells, "Alignment by maximization of mutual information," *J. Comput. Vision*, vol. 24, no. 2, pp. 137–154, 1997.

[18] W. M. Wells, P. Viola, H. Atsumini, S. Nakajima, and R. Kikinis, "Multimodal volume registration by maximization of mutual information," *Med. Image Anal.*, vol. 1, no. 1, pp. 35–51, 1996.

[19] S. Lankton and A. Tannenbaum, "Localizing region-based active contours," *IEEE Trans. Image Process*, vol. 17, no. 11, pp. 2029–2039, Nov. 2008.

[20] M. Goryawala, M. R. Guillen, S. Gulec, T. Barot, R. Suthar, R. Bhatt, A. McGoron, and M. Adjouadi, "A new 3D liver segmentation method with parallel computing for selective internal radiation therapy," *IEEE Trans. Inf. Technol. Biomed.*, vol. 16, no. 1, pp. 62–69, Jan. 2012.

[21] H. Li and A. Yezzi, "Local or global minima: Flexible dual-front active contours," *IEEE Trans. Pattern Anal. Mach. Intell.*, vol. 29, no. 1, pp. 1–14, Jan. 2007.

[22] P. Perona and J. Malik, "Scale-space and edge-detection using anisotropic diffusion," *IEEE Trans. Pattern Anal.*, vol. 12, no. 7, pp. 629–639, Jul. 1990.

[23] B. Meihua, G. Siyu, T. Qiu, and Z. Fan, "Optimization of the bwmorph Function in the MATLAB image processing toolbox for binary skeleton computation," in *Proc. Int. Conf. Comput. Intell. Nat. Comput.*, Wuhan, China, 2009, pp. 273–276.

[24] B. F. Jones and P. Plassmann, "Digital infrared thermal imaging of human skin," *IEEE Eng. Med. Biol. Mag.*, vol. 21, no. 6, pp. 41–48, Nov./Dec. 2002.

[25] F. Candocia and M. Adjouadi, "A similarity measure for stereo feature matching," *IEEE Trans. Image Process.*, vol. 6, no. 10, pp. 1460–1464, Oct. 1997.

[26] M. Adjouadi and F. Candocia, "A stereo matching paradigm based on the Walsh transformation," *IEEE Trans. Pattern Anal. Mach. Intell.*, vol. 16, no. 12, pp. 1212–1218, Dec. 1994.

[27] P. J. Flynn, K. W. Bowyer, and P. J. Phillips, "Assessment of time dependency in face recognition: An initial study," in *Proc. Audio- and Video-Based Biometric Person Authentication*, 2003, pp. 44–51.

[28] X. Chen, P. J. Flynn, and K. W. Bowyer, "Visible -light and infrared face recognition," in *Proc. ACM Workshop Multimodal User Authentication*, Dec. 2003, pp. 48–55.

Authors' photographs and biographies not available at the time of publication.